ACS NANO
Cite This: ACS Nano XXXX, XXX, XXX−XXX
www.acsnano.org

ARTICLE

Influence of Homopolymer Addition in Templated Assembly of Cylindrical Block Copolymers

Jan Doise,*[,†,‡] Cody Bezik,[§] Masafumi Hori,[∥] Juan J. de Pablo,[§] and Roel Gronheid[‡,⊥]

[†]Department of Electrical Engineering (ESAT), KU Leuven, Kasteelpark Arenberg 10, B-3001 Heverlee, Belgium
[‡]imec, Kapeldreef 75, B-3001 Heverlee, Belgium
[§]Institute for Molecular Engineering, University of Chicago, 5747 South Ellis Avenue, Chicago, Illinois 60637, United States
[∥]JSR Micro N.V., Technologielaan 8, B-3001 Leuven, Belgium

Supporting Information

ABSTRACT: Templated assembly of cylindrical block copolymers provides a promising strategy for patterning holes at the nanoscale. However, remaining challenges include the ability to achieve defect-free patterns and to generate architectures useful for device patterning. The aim of this work is to gain insight into the influence of homopolymer addition on the assembly of a cylindrical block copolymer in confined space. To do so, a concerted examination that relies on experiments and simulations is carried out for different block copolymer/homopolymer blends. It is shown that by adding a majority block homopolymer with low molecular weight (compared to the blocks that make up the block copolymer), the pattern quality is significantly improved and a larger defect-free window is obtained in terms of template dimensions for two-hole features in elliptical confinements. The redistribution of the homopolymer chains effectively enables the assembly of two cylinders, despite the geometrical mismatch between the elliptical shape of the confinement and the natural hexagonal ordering of the unguided block copolymer. Monte Carlo simulations show that the homopolymer segregates to the spaces in the template that are entropically unfavorable for the block copolymer. This work serves to highlight the importance of optimizing block copolymer formulation.

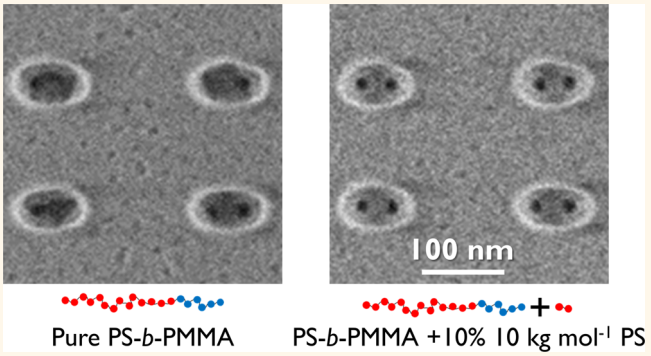

KEYWORDS: *directed self-assembly, block copolymer, homopolymer, grapho-epitaxy, template, confinement, blend*

Directed self-assembly of block copolymers is an effective strategy for the creation of nanoscale patterns and devices.[1−3] While numerous experimental articles have been published on guiding the assembly of pure block copolymer systems, reports of directed assembly of block copolymer/homopolymer blends have been less common. Stoykovich *et al.*[4] showed that blends of lamellae forming diblock copolymers and homopolymers enable assembly of nonregular device-oriented line structures on chemically nanopatterned substrates. In that work, it was shown that redistribution of homopolymer facilitates the defect-free assembly in locations where the domain dimensions deviate substantially from those of the pure block copolymer. In addition, several manuscripts have considered undirected thin-film assemblies of diblock copolymer/homopolymer blends and have yielded insights into the morphological behavior of blends and the distribution of homopolymer chains within the copolymer domain.[5−10] In particular, Chevalier *et al.*[11] showed that these mixtures exhibit interesting characteristics, such as the ability to assemble into thicker defect-free films, improved kinetics of defects annihilation, and larger grain sizes compared to pure diblock copolymers. Finally, there are also reports on enhancement of the (directed) self-assembly kinetics of a block copolymer by blending in comparively short copolymer chains.[12−15]

Although a limited number of reports exist,[16−18] the influence of homopolymer addition to a cylinder-forming diblock copolymer on its assembly in a confined geometry has not been systematically investigated. Such templated assembly, also called grapho-epitaxy, is a process of considerable interest for the semiconductor industry, as it is considered a potential solution for patterning randomly distributed holes with size and

Received: November 2, 2018
Accepted: March 14, 2019
Published: March 14, 2019

DOI: 10.1021/acsnano.8b08382
ACS Nano XXXX, XXX, XXX−XXX

periodicity beyond the reach of optical lithography.[19−21] One of the challenges in the implementation of this approach is to achieve defect-free patterns and the ability to generate architectures useful for device patterning.[1] The use of feature multiplication in the form of two-hole features (called doublets, as illustrated in Figure 1), next to plain hole shrink structures

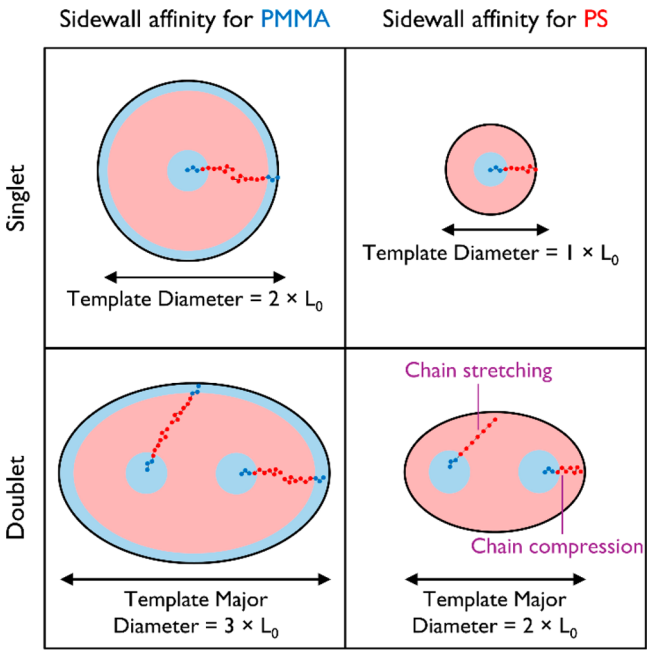

Figure 1. Schematic illustration of arrangement of PS-*b*-PMMA block copolymer chains inside singlet and doublet templates with different sidewall affinity. The appropriate confinement dimensions for templates with affinity for the majority block, PS, are significantly smaller, which allows for more dense patterns to be generated.

(singlets), is required for this method to be advantageous.[18,22,23] Bekaert *et al.* have shown that the template sidewalls should have an affinity for the majority block in order to be able to generate sufficiently dense layouts for device manufacturing (as illustrated in Figure 1).[22] However, in earlier experimental work with poly(styrene-*block*-methyl methacrylate) (PS-*b*-PMMA), we have observed a smaller process window in terms of template dimensions for doublets in elliptical templates with sidewall affinity for the majority block (PS), compared to doublets in templates with sidewall affinity for the minority block (PMMA).[24] This was hypothesized to be caused by a mismatch between the natural hexagonal ordering of the block copolymer and the elliptical geometry of the template, which causes an entropic penalty due to local stretching and compression of chains as visualized in Figure 1. In the case of a sidewall with affinity for PMMA, this mismatch is significantly reduced by the larger number of available chains. In addition, for singlets, the circular geometry of the templates suits the natural chain conformations and packing of a cylindrical block copolymer, regardless of sidewall affinity, and large process windows are generally observed.

One way to address such issues is to generate peanut-shaped templates that better match the natural ordering of the chains, but, at these dimensions, this is not possible with 193 nm immersion lithography and requires instead a process such as e-beam or extreme ultraviolet lithography.[25] In this work, we present an alternative approach based on adjusting the block copolymer formulation. We build on the same principles as those reported in Stoykovich *et al.*[4] (*i.e.*, adding homopolymer to enable directed assembly that deviates from the natural ordering) and apply them to the templated assembly of a cylindrical block copolymer. A systematic investigation is carried out of the influence of homopolymer addition to a cylindrical block copolymer on the self-assembly in a confined geometry. It is shown that by adding majority block homopolymer with low molecular weight compared to that of the blocks that make up the copolymer, the pattern quality for doublets is significantly improved, and a substantially larger defect-free window is achieved in terms of template dimensions.

RESULTS AND DISCUSSION

The block copolymer employed in this study is cylindrical PS-*b*-PMMA, with molecular weight M_n = 66.5 kg mol^{-1} for PS and M_n

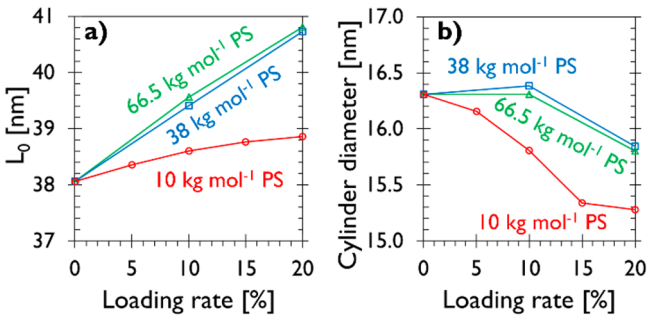

Figure 2. L_0 (a) and PMMA cylinder diameter (b) of PS-*b*-PMMA blended with PS homopolymer as a function of PS homopolymer loading rate (in weight %) and molecular weight. L_0 and cylinder diameter were measured from SEM images of unguided assembly. Experimental details can be found in the methods.

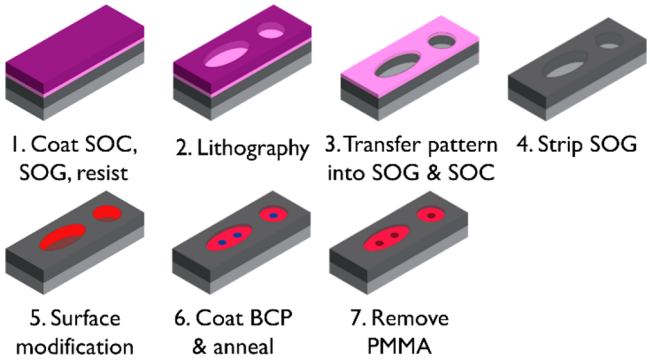

Figure 3. Schematic overview of the process flow used for templated assembly in this work.

= 28.5 kg mol^{-1} for PMMA. Block copolymer/homopolymer blends were prepared by adding PS homopolymer, with three different molecular weights and at different loading rates. The unguided domain spacing, L_0, and cylinder diameter of these blends are shown in Figure 2. It should be noted that for cylindrical phase block copolymers, there exists ambiguity in the literature regarding the definition of the domain spacing L_0: It may refer to either the center-to-center intercylinder distance or to the row-to-row distance, which is equal to $\sqrt{3}/2$ times the center-to-center value. We use the center-to-center distance, as this is the relevant value for determining commensurate template dimensions in the common grapho-epitaxy structures illustrated in Figure 1.

DOI: 10.1021/acsnano.8b08382
ACS Nano XXXX, XXX, XXX−XXX

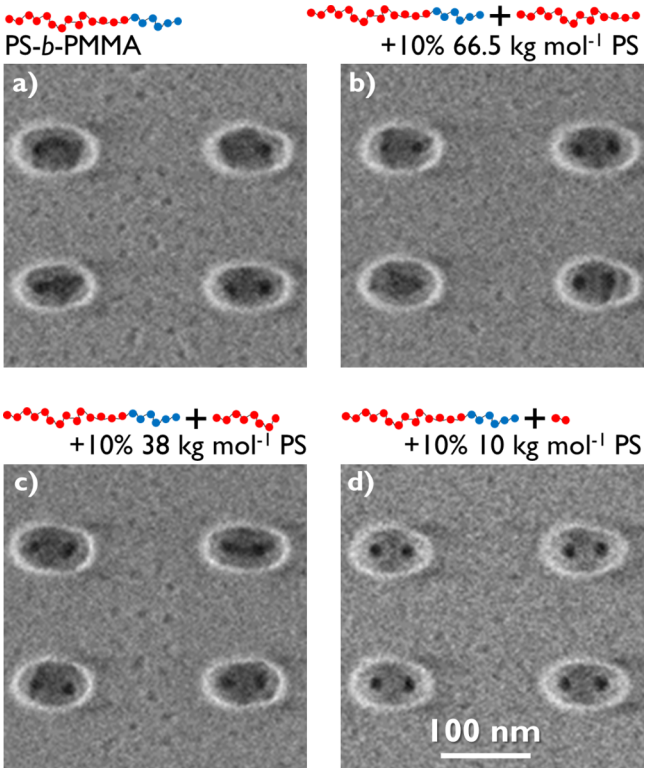

Figure 4. Representative SEM images after PMMA removal of (a) pure PS-*b*-PMMA and PS-*b*-PMMA with the addition of (b) 10% 66.5 kg mol^{-1} PS, (c) 10% 38 kg mol^{-1} PS, and (d) 10% 10 kg mol^{-1} PS inside elliptical templates with sidewall affinity for PS and average major × minor diameter 85 × 52 nm. Image size is 338 × 338 nm. A larger field of view of the same images can be found in Figure S2 in the Supporting Information.

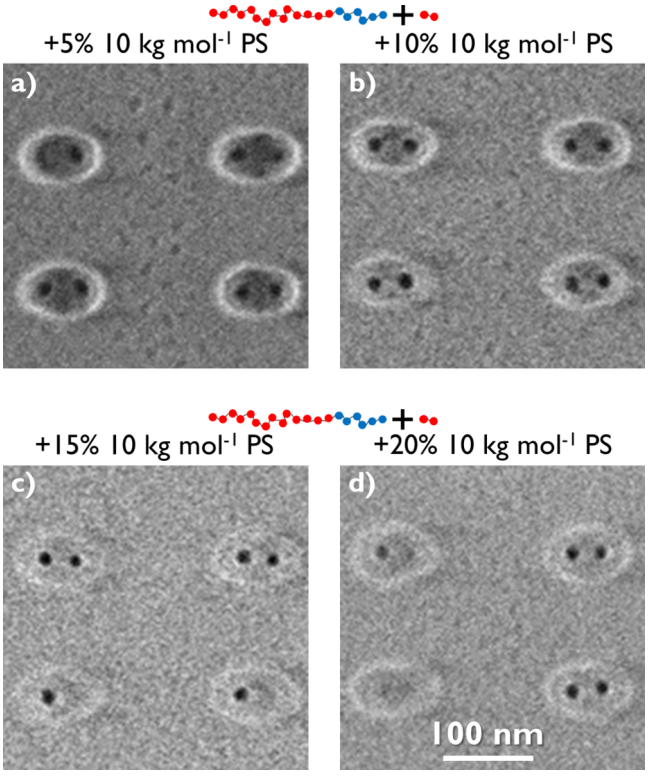

Figure 5. Representative SEM images after PMMA removal of PS-*b*-PMMA with the addition of (a) 5%, (b) 10%, (c) 15%, and (d) 20% 10 kg mol^{-1} PS inside elliptical templates with sidewall affinity for PS and average major × minor diameter 85 × 52 nm. Image size is 338 × 338 nm. A larger field of view of the same images can be found in Figure S4 in the Supporting Information.

With increasing 66.5 kg mol^{-1} or 38 kg mol^{-1} PS homopolymer content, L_0 increases considerably due to expansion of the PS domain, while the size of the PMMA domain does not change significantly for loading rates up to 10%. The contrary is true for the lower molecular weight of 10 kg mol^{-1}, where L_0 only slightly increases, but the PMMA domain diameter shrinks significantly upon addition of PS homopolymer. This agrees with earlier findings from Hashimoto *et al.* and Mayes *et al.*,[6,8] who observed that when a homopolymer with molecular weight comparable to that of the block is added to a lamellar copolymer, the homopolymer is confined to the corresponding copolymer domain, with a distribution that peaks at the center of the domain. This results in an increase of the domain spacing due to an expansion of the PS domain, while the PMMA domain remains unchanged. In the case of significantly lower molecular weight, intermixing of the homopolymer chains with the copolymer block is more entropically favored, and the homopolymer is more uniformly distributed within the domain. Swelling of the PS blocks by short homopolymer chains now results in a larger average distance between PS-PMMA junction points along the interface, producing a shrink of the adjacent PMMA domains that helps preserve a uniform density.

Figure 3 shows a schematic overview of the process flow used for templated assembly in this work. This flow has been discussed extensively before[24] and is based on the fabrication of templates consisting of spin-on-carbon (SOC) hard-mask material through the use of conventional 193 nm immersion lithography and dry etch techniques for patterning. Before the block copolymer/homopolymer blend is applied, the surface chemistry of the prepattern is tailored using a polymer brush. In this work, two variations of surface modification are used that result in a nonpreferential bottom surface and sidewalls with affinity for PS and PMMA, respectively. Note that the different block copolymer/homopolymer blends are spin-coated at identical film thickness (as measured on a wafer without topography), but the resulting template fill (*i.e.*, the local film thickness inside the topographic confinement) may be different depending on the polymer mobility of the blend and the template pattern density, that is, the percentage of area the templates occupy. The closer the templates are packed together, the higher the template pattern density and the lower the resulting template fill level.[26] By inspecting fields with different pattern density, the influence of template fill on the resulting morphology can be evaluated.

Figure 4 shows representative scanning electron microscope (SEM) images of the assembly of pure PS-*b*-PMMA as well as PS-*b*-PMMA blended with 10% of PS homopolymer of different molecular weights inside elliptical templates with sidewall affinity for PS. The pure PS-*b*-PMMA shows unstable assembly, with defects such as deformed or (partly) parallel oriented cylinders occurring predominantly. Upon addition of the homopolymer with larger molecular weight (66.5 kg mol^{-1} and 38 kg mol^{-1}), only minor improvements are observed. This should be contrasted with the considerable improvements that are obtained in pattern quality for the blend with 10 kg mol^{-1} PS (Figure 4d). The presence of the short PS homopolymer chains effectively relaxes the geometrical

DOI: 10.1021/acsnano.8b08382
ACS Nano XXXX, XXX, XXX−XXX

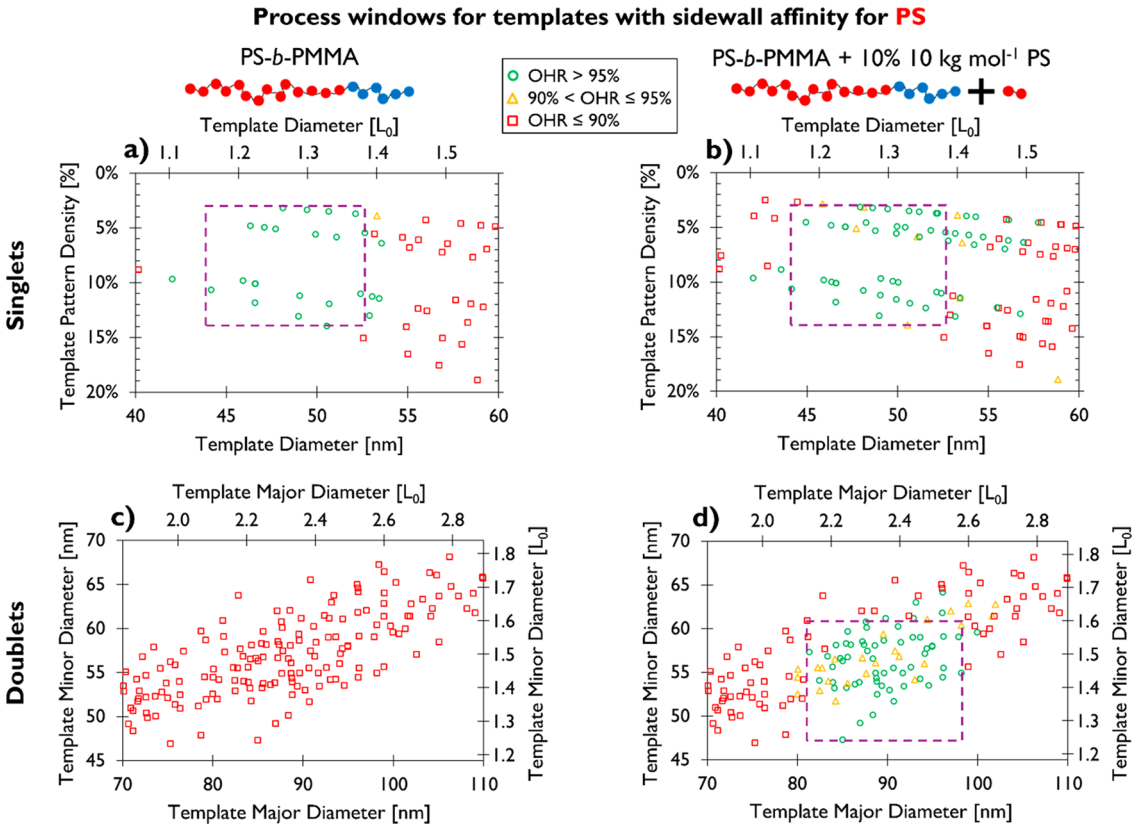

Figure 6. Process windows for templates with affinity for PS. (a) Process window for singlets with pure PS-*b*-PMMA as a function of template diameter and pattern density. (b) Process window for singlets with PS-*b*-PMMA + 10% 10 kg mol^{-1} PS as a function of template diameter and pattern density. (c) Process window for doublets with pure PS-*b*-PMMA as a function of template major and minor diameter. (d) Process window for doublets with PS-*b*-PMMA + 10% 10 kg mol^{-1} PS as a function of template major and minor diameter. Green circles correspond to an OHR > 95%, orange triangles correspond to 90% < OHR ≤ 95%, and red squares correspond to an OHR ≤ 90%.

constraints placed on the block copolymer at the boundaries. This enables the desired morphology consisting of two clearly defined cylinders (which is not stable for the pure PS-*b*-PMMA due to the high degree of local stretching and compression), as illustrated in Figure 1. The available short homopolymer chains can redistribute within the template and occupy the spaces that are unfavorable for the block copolymer from an entropic viewpoint. In addition, from the SEM signal intensity inside the templates in Figure 4d, one can appreciate that the template fill is higher for the blend with 10% 10 kg mol^{-1} (line profiles of the SEM signal intensity can be found in Figure S1 in the Supporting Information). This can be attributed to the lower molecular weight homopolymer, which acts as a plasticizer by lowering the glass transition temperature of the PS domain,[27,28] and thus increases the overall mobility of the polymer blend. As a result, more transport of polymer material into the templates occurs during the thermal anneal step. It should be noted that while Figure 4 only shows results for a specific template size and pattern density, a large range of template dimensions and pattern densities were investigated in our experiments, without ever observing a single defect-free image for the pure PS-*b*-PMMA or blends with 66.5 kg mol^{-1} and 38 kg mol^{-1} homopolymer. A more detailed discussion on the results with the blend with 10 kg mol^{-1} will follow below.

To verify that the defective morphologies found for pure PS-*b*-PMMA in Figure 4 are not a result of slower kinetics compared to the blend with 10% 10 mol kg^{-1} PS, samples with increased annealing times were also prepared. As the defective morphologies persist for the longer annealing time without an increase in the number of defect-free assemblies (SEM images shown in Figure S3 in the Supporting Information), it can be assumed that for pure PS-*b*-PMMA these defective states are at least as stable as the desired morphology, within the practical time scales for assembly.

Figure 5 shows SEM images of the assembly of PS-*b*-PMMA blended with 10 kg mol^{-1} PS with increasing concentration of the homopolymer in identical templates to those used in Figure 4.

An optimum in terms of assembly quality can be observed at +10% 10 kg mol^{-1} PS. At a loading rate of 5%, many defects are still observed, as there are not enough short PS chains available to relax the geometric constraints. In addition, the assembly of blends with higher loading rates shows a lot of closed or missing holes. We hypothesize that, in this case, excess PS homopolymer may segregate to the top surface (as also observed by Mayes *et al.*[6] for unguided assembly of lamellar PS-*b*-PMMA) thanks to its lower surface energy[29] and cause a skin layer on top of the PMMA domains. The fact that not all holes are missing are attributed to local variations in template dimensions and resulting fill level (which have been characterized before)[26] due to the lithography and etch processes used to fabricate the prepattern.

Figure 6 shows process windows for templates with sidewall affinity for PS using pure PS-*b*-PMMA as well as using the blend with 10% 10 kg mol^{-1} PS. The process windows depict the area of defect-free assembly for a given block copolymer-homopol-

DOI: 10.1021/acsnano.8b08382
ACS Nano XXXX, XXX, XXX−XXX

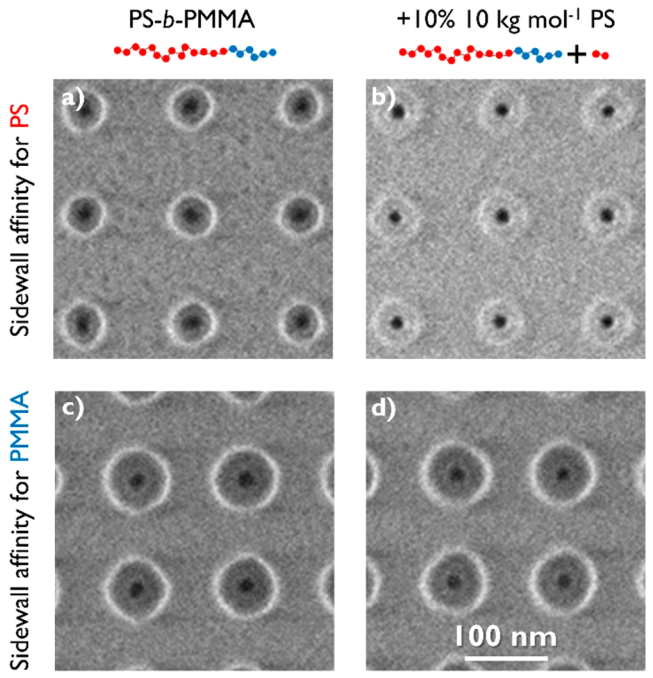

Figure 7. Representative SEM images after PMMA removal of (a, c) pure PS-*b*-PMMA and (b, d) PS-*b*-PMMA + 10% 10 kg mol^{-1} PS inside circular templates with (a, b) sidewall affinity for PS and average diameter 50 nm and (c, d) sidewall affinity for PMMA and average diameter 70 nm. Image size is 338 × 338 nm. A larger field of view of the same images can be found in Figure S7 in the Supporting Information.

ymer blend, based on the open hole rate (OHR) after PMMA removal, as judged from top-down SEM imaging. For singlets, the process windows are plotted as a function of template diameter and template pattern density. As mentioned earlier, by inspecting fields with different pattern density, the influence of template fill on the resulting morphology can be evaluated. For doublets, the process windows are plotted as a function of template major and minor diameter (the same data plotted as a function of template area and template pattern density can be found in Figure S5 in the Supporting Information to evaluate the influence of the template fill). Regarding singlets, no significant difference in terms of process window size is observed between pure PS-*b*-PMMA (Figure 6a) and PS-*b*-PMMA blended with 10% 10 kg mol^{-1} PS (Figure 6b). As the circular geometry of the singlet templates matches the natural chain conformations and packing of cylindrical PS-*b*-PMMA (as illustrated in Figure 1), it does not impose any geometric frustration on the assembly, and stable formation of perpendicular PMMA domains is possible without addition of homopolymer. The center of the process window at 48 nm or ~1.3 × L_0 approximately corresponds to the 1 × L_0 scheme for singlets with sidewall affinity for PS, as illustrated in Figure 1. As the template dimensions listed are measured in SOC, the confinement further shrinks by ~10 nm due to the polymer brush used for surface modification, although the polymer brush may interdigitate with the block copolymer and, as such, does not act as a hard boundary. In the representative SEM images (Figure 7a,b) from the center of the process window, it can be seen that while there is a big contrast difference due to a difference in template fill (line profiles of the SEM signal intensity can be found in Figure S6 in the Supporting Information), similar cylindrical PMMA domains are observed in each case.

Regarding doublets, as mentioned earlier, no defect-free images are found for the pure PS-*b*-PMMA over a wide range of elliptical templates (Figure 6c). On the other hand, a large process window is observed for PS-*b*-PMMA blended with 10% 10 kg mol^{-1} PS (Figure 6d). The center of the process window (at template major diameter ~2.3 × L_0) corresponds to the ~2 × L_0 scheme for doublets with sidewall affinity for PS, as depicted in Figure 1 (again taking the shrink caused by the polymer brush into account).

It should be noted that only periodic arrays of singlets and doublets are studied in this work, while an important possible application for templated self-assembly of cylindrical block copolymer is to generate aperiodic patterns commonly found in layout of logic devices, using a combination of singlets and doublets. In previous work,[18] we have demonstrated the simultaneous patterning of singlets and doublets in a representative, aperiodic layout employing the same blend of PS-*b*-PMMA with 10% 10 kg mol^{-1} PS.

Figure 8 shows process windows for templates with sidewall affinity for PMMA. Regarding singlets, consistent with the process windows for templates with sidewall affinity for PS, no significant difference in terms of process window size is observed between pure PS-*b*-PMMA (Figure 8a) and PS-*b*-PMMA blended with 10% 10 kg mol^{-1} PS (Figure 8b); this is due to the circular geometry, which matches the natural chain conformations of the cylindrical block copolymer. The center of the process window (at template diameter ~1.8 × L_0) corresponds roughly to the ~2 × L_0 scheme for singlets with sidewall affinity for PMMA, as illustrated in Figure 1. In the representative SEM images (Figure 7c,d) from the center of the process window, it can be seen in that almost identical cylindrical PMMA domains are observed in each case. No difference in template fill level is observed between the pure PS-*b*-PMMA and the blend with 10% 10 kg mol^{-1} PS. We hypothesize that for the templates fabricated with this flow, the polymer mobility on the unpatterned area is already high for pure PS-*b*-PMMA (which is apparent from the lack of polymeric material on top of this area), and the plasticizing effect of the low molecular weight homopolymer has little additional impact on the template fill level.

Concerning doublets, a sizable process window is observed for pure PS-*b*-PMMA (Figure 8c) in templates with affinity for PMMA. In this case, the area of the template is three times larger compared to the case for templates with affinity for PS (see Figure 1) and thus fits ~3 times as many polymer chains. As schematically depicted in Figure 1, this has a significant impact on the packing frustration, as (compared to the situation with sidewall affinity for PS) there are no zones where the chains now have to be strongly stretched or compressed, which are very unfavorable from an entropic viewpoint. Still, the process window for PS-*b*-PMMA blended with 10% 10 kg mol^{-1} PS (Figure 8d) is significantly larger. At the edges of the process window, as the template geometry becomes less commensurate with the natural packing, the pure PS-*b*-PMMA assembles into less desired morphologies, such as doublets with a horizontal bridge at the top (highlighted in Figure 9c), where stable perpendicular cylinders are still observed for PS-*b*-PMMA blended with 10% 10 kg mol^{-1} PS (Figure 9d). The center of the process windows corresponds to the ~3 × L_0 scheme for doublets with sidewall affinity for PMMA, as illustrated in Figure 1.

In order to provide evidence that the improved assembly upon PS homopolymer addition is caused by redistribution of

DOI: 10.1021/acsnano.8b08382
ACS Nano XXXX, XXX, XXX−XXX

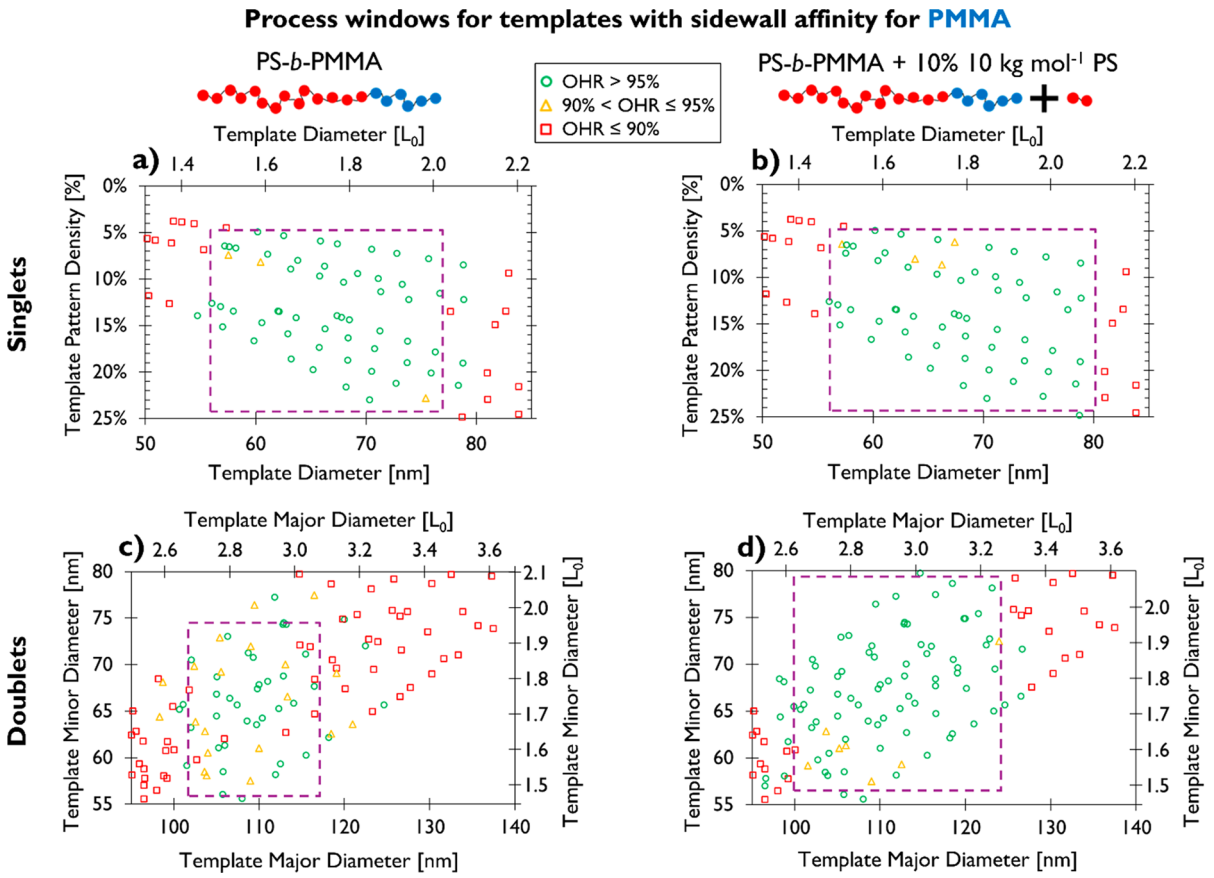

Figure 8. Process windows for templates with affinity for PMMA. (a) Process window for singlets with pure PS-*b*-PMMA as a function of template diameter and pattern density. (b) Process window for singlets with PS-*b*-PMMA + 10% 10 kg mol^{-1} PS as a function of template diameter and pattern density. (c) Process window for doublets with pure PS-*b*-PMMA as a function of template major and minor diameter. (d) Process window for doublets with PS-*b*-PMMA + 10% 10 kg mol^{-1} PS as a function of template major and minor diameter. Green circles correspond to an OHR > 95%, orange triangles correspond to 90% < OHR ≤ 95%, and red squares correspond to an OHR ≤ 90%.

homopolymer chains, Monte Carlo (MC) simulations of the blends considered in our experiments were performed using a theoretically informed coarse-grained model.[30] Figure 10 shows several morphology diagrams for doublet assembly as a function of template major and minor diameter, as determined by the MC simulations. The simulation conditions are analogous to those considered in the experimental process windows shown in Figures 6 and 8. The simulated morphologies are grouped into five main categories: separated doublets, bridged doublets, missing cylinder(s), crescents, and elongated bars. A separated doublet is the desired morphology and hence is labeled green in Figure 10. While a bridged doublet is considered a nonideal morphology, it may still be useful for patterning purposes, as it likely results in two separate holes after a typical pattern transfer process into an underlying layer. As such, it is marked in orange. Missing cylinder(s), crescent-like shapes, and elongated bars are marked red, as they are unlikely to be useful for patterning purposes. Representative examples of each type of observed morphology are shown in Figure 11.

In agreement with our experimental data, it can be seen in that a stable separated doublet morphology is unlikely to result from the pure block copolymer in templates with sidewall affinity for PS (Figure 10a). Furthermore, the larger open hole rates observed experimentally for the blend with +10 kg mol^{-1} PS are consistent with the simulated morphology diagram for this blend (Figure 10b). The predicted range in terms of template dimensions over which stable separated doublets corresponds well with the experimental process window.

The experimentally observed widening of the process window upon addition of homopolymer in templates with sidewall affinity for PMMA is also in agreement with data obtained through simulations (Figure 10c,d). Furthermore, precisely as shown experimentally in the SEM images (Figure 9c), the bridged doublet morphology is often observed for the pure block copolymer (Figure 10c). In contrast, the homopolymer/block copolymer blend shows an increased number of separated doublets (Figure 10d).

Small disagreements between the experimental results and the MC simulations regarding the precise regions of good assembly may be the result of kinetically trapped metastable structures.[31] Areas where the simulations predict a defective state, but where a good open hole rate is observed experimentally, are likely to correspond to regions where the separated doublet morphology is dominant in terms of probability, but where defective metastable states arise along the assembly pathway, leading to local free energy traps for a specific simulation trajectory. For large numbers of assemblies, and with experimentally accessible thermal annealing times, the experimental systems have in general an opportunity to overcome the free energy barriers associated with the metastable states. The opposite scenario, where the simulation predicts a separated doublet, but the experiments show reduced open hole rates due to kinetically trapped states, is likewise possible. Note that the relevant

DOI: 10.1021/acsnano.8b08382
ACS Nano XXXX, XXX, XXX−XXX

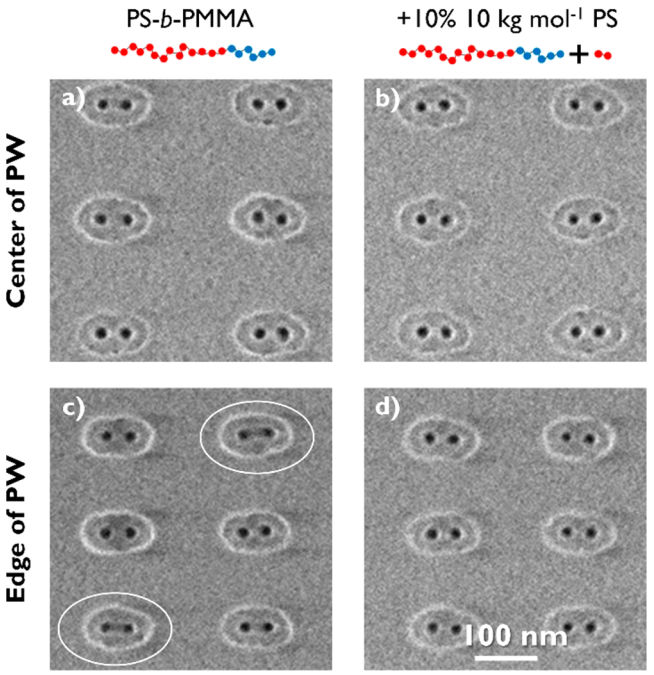

Figure 9. Representative SEM images after PMMA removal of (a, c) pure PS-*b*-PMMA and (b, d) PS-*b*-PMMA + 10% 10 kg mol^{-1} PS inside elliptical templates with sidewall affinity for PMMA and (a, b) average major × minor diameter 110 × 67 nm, in the center of the process window (PW) and (c, d) 106 × 62 nm, at the edge of the PW. In (c), occurrences of the bridged doublet morphology are encircled. Image size is 450 × 450 nm. A larger field of view of the same images can be found in Figure S8 in the Supporting Information.

pathways for assembly have been discussed in our previous work, and they do reveal the appearance of local free energy minima separated by free energy barriers.[32] We additionally note that, in the case of PMMA wetting sidewalls, there appears to be a systematic shift in the process windows in terms of template major diameter. The simulations predict the desired assembly to occur in ∼10 nm larger templates than those observed experimentally. We hypothesize that the simulations may overestimate the thickness of the PMMA wetting layer at the sidewall. This layer can be as thick as 8 nm in the simulations, but, paradoxically, it is too thin in practice to be perceptible with cross-sectional TEM methods.[24,33] An overestimation of this thickness effectively results in a shift toward larger confinements for the simulations.

Figure 12 serves to provide a better understanding of how the homopolymer chains help stabilize the desired doublet morphology. The homopolymer density in a template in which the simulations predict a stable separated doublet is plotted using a parameter Φ_2, which takes on the value of zero when the density of the homopolymer in a grid cell is exactly the average homopolymer density, and adopts values greater than zero when it is larger than the average density. From this figure, it becomes clear that PS homopolymer preferentially segregates to the upper and lower section of the elliptical templates—exactly the regions where the block copolymer chains would need to be stretched to fit the template.

CONCLUSIONS

The influence of PS homopolymer addition in templated assembly of cylindrical PS-*b*-PMMA has been investigated through a combination of experiments and simulations. Considerably improved pattern quality and larger process windows in terms of template dimensions for two-hole features in elliptical templates can be achieved by adding PS homopolymer of low molecular weight compared to that of the blocks that make up the copolymer. The mismatch between the natural hexagonal ordering of the block copolymer and the elliptical geometry is effectively reduced by the redistribution of the short homopolymer chains. MC simulations confirm that the homopolymer segregates to the spaces in the template that are entropically unfavorable for the block copolymer. This effect is more pronounced for a prepattern with sidewalls with affinity for PS. Since a circular template for one-hole features matches the natural packing of a cylindrical block copolymer, it does not impose any geometric frustration on the assembly. As a result, there is no benefit of homopolymer addition for these one-hole features. This work underscores the importance of optimizing block copolymer formulation. While the work herein was focused on improving the pattern quality of templated assembly of cylindrical block copolymers in elliptical templates, the same general principles can be applied to a wide range of block copolymers and geometries to create various patterns and devices.

METHODS

Materials. Cylindrical phase poly(styrene-*block*-methyl methacrylate) (PS-*b*-PMMA) with M_n = 66.5 kg mol^{-1} for PS and M_n = 28.5 kg mol^{-1} for PMMA and PS homopolymer with M_n = 10 kg mol^{-1}, M_n = 38 kg mol^{-1}, and M_n = 66.5 kg mol^{-1} was synthesized by JSR Micro. The PS-*b*-PMMA was blended with the different PS homopolymers at various weight % and dissolved in propyl glycol methyl ether acetate.

Guiding Template Fabrication Process. Guiding templates used in work were fabricated on 300 mm silicon wafers as reported before[24] and consist of a patterned spin-on-carbon layer, of which the surface chemistry has been tailored for subsequent self-assembly. Flow #2 and #3 (as previously described in detail)[24] were used to fabricate templates with a nonpreferential bottom surface and sidewalls with affinity for respectively PMMA and PS. Different template dimensions and pattern densities could be generated on the same wafer by varying lithographic mask dimensions and exposure dose.

Grapho-Epitaxy-Directed Self-Assembly Process. Block copolymer coating and annealing was done on a Tokyo Electron Clean Track Act 12. The block copolymer or blend was spin-coated from solution and thermally annealed under a nitrogen atmosphere at 250 °C for 5 min unless otherwise noted. The film thickness (as measured with a KLA Tencor SCD-100 ellipsometer on a wafer without topography after using an identical coating process) employed was 8.5 nm for templates with affinity for PS and 11 nm for templates with affinity for PMMA. The PMMA domains were removed by exposure to ultraviolet radiation followed by an isopropyl alcohol rinse on a Tokyo Electron Clean Track Lithius Pro Z.

Grapho-Epitaxy Characterization. Wafers were analyzed using a Hitachi CG-5000 or CG-6300 top-down critical dimension scanning electron microscope (CD-SEM). For measuring template dimensions, SEM images with field of view of 675 nm × 675 nm were analyzed with Robust Edge Detection (RED) software from Hitachi. All template dimensions reported are measured prior to surface modification of the spin-on-carbon layer. While the polymer brushes applied for surface modification reduce the template diameter (as measured by CD-SEM) by ∼6 nm (for flow #2) and ∼10 nm (for flow #3), these polymer brushes can interdigitate with the block copolymer blend during self-assembly and as such do not act as an absolute boundary for the assembly. To determine the open hole rates reported in Figures 6 and 8, SEM images with a field of view of 1.35 × 1.35 μm taken after PMMA removal were manually inspected. When the correct number of open holes were observed in a template without obvious deformations, this was counted as an open hole. In case there were either missing, extra, or

DOI: 10.1021/acsnano.8b08382
ACS Nano XXXX, XXX, XXX−XXX

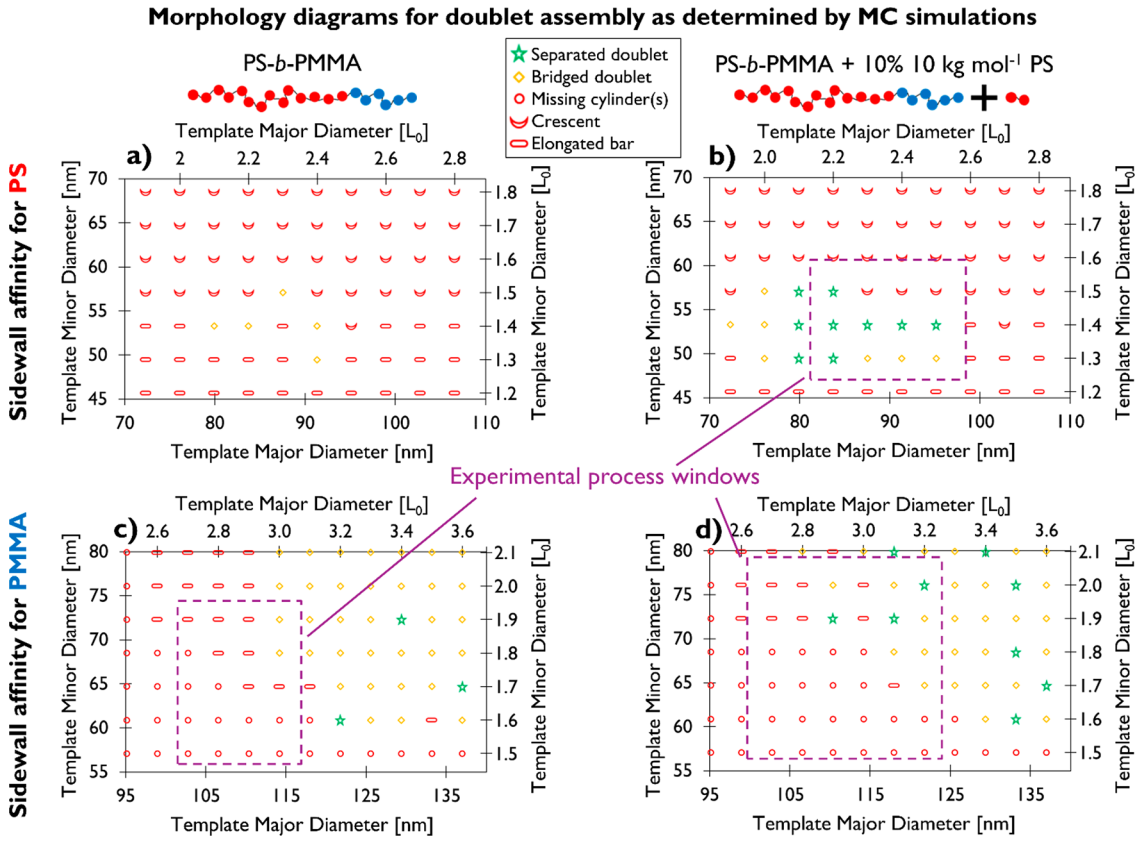

Figure 10. Morphology diagrams for doublet assembly as a function of template major and minor diameter as determined by MC simulations. (a) Morphology diagram for pure PS-*b*-PMMA in templates with sidewall affinity for PS. (b) Morphology diagram for PS-*b*-PMMA + 10% 10 kg mol^{-1} PS in templates with sidewall affinity for PS. (c) Morphology diagram for pure PS-*b*-PMMA in templates with sidewall affinity for PMMA. (d) Morphology diagram for PS-*b*-PMMA + 10% 10 kg mol^{-1} PS in templates with sidewall affinity for PMMA. Green stars correspond to separated doublets, orange diamonds correspond to bridged doublets, and red markers correspond to defective morphologies such as missing cylinder(s), crescents, and elongated bars. For sake of comparison, the experimentally determined process windows from Figures 6 and 8 are depicted (dashed line rectangle).

deformed holes observed in a template, this was counted as a closed hole.

Unguided Self-Assembly and Characterization. To determine unguided center-to-center domain spacing L_0 and PMMA domain diameter of the different samples used (Figure 2), the surface of a silicon wafer was modified with the same random copolymer brush as used for flow #2 (as described in ref 24) to promote perpendicular orientation. Next, the block copolymer or blend was spin-coated from solution at a film thickness of 15 nm and annealed under a nitrogen atmosphere at 250 °C for 5 min. To increase image contrast, the PMMA domains were removed by exposure to ultraviolet radiation followed by an isopropyl alcohol rinse. To measure L_0 and PMMA cylinder diameter, SEM images with fields of view of 675 × 675 nm and 337 × 337 nm were analyzed with RED software from Hitachi. Reported values are averages of 16 images collected across the wafer.

Computational Simulations. The model used here is a theoretically informed coarse grained (TICG) model, relying on discretizing full block copolymer chains into n Gaussian chains of N beads connected by springs.[30,34,35] This model has previously been shown to be in good agreement with experimental results.[36,37] In this model, the energy associated with the polymer bonds is expressed as

$$\frac{H_b}{k_BT} = \frac{3}{2}\sum_{i=1}^{n}\sum_{s=1}^{N-1}\frac{(N-1)[r_i(s+1)-r_i(s)]^2}{R_e^2}$$

where the sth bead on the ith chain has position $r_i(s)$. R_e is the end-to-end distance of the polymer chains; typically, a unit system is adopted for the simulations where the end-to-end distance is unity. Additionally, k_B is the Boltzmann constant. The nonbonded interactions consist of a Flory–Huggins type interaction, quantifying the incompatibility between the two types of monomers and a term relating to the finite compressibility of the melt. The energy associated with nonbonded interactions is given as

$$\frac{H_{nb}}{k_BT} = \sqrt{N}\int_V \frac{dr}{R_e^3}\left[\chi N\phi_A\phi_B + \frac{kN}{2}(1-\phi_A-\phi_B)^2\right]$$

where $\sqrt{N} = \frac{\rho_0 R_e^3}{N}$, the interdigitation number, is an estimate of the number of chains a given chain interacts with (ρ_0 is the average bulk number density of beads). The parameter χ is the familiar Flory–Huggins parameter, and κ^{-1} is proportional to the melt compressibility. Each term $\phi(r)$ is a function of the local density of each type of bead; these densities are calculated by a particle-to-mesh scheme, where a grid (each grid cell is a cube with side length ΔL) is overlaid on the system and each bead is assigned to its nearest grid (PM0). Full details of the model are available in Detcheverry *et al.*[30]

The confinement is modeled as hard walls; the sidewall and bottom substrate interact with the polymer according to the term

$$\frac{H_s}{k_BT} = \sum_{i=1}^{nN} f_s(x,y,K)\frac{\Lambda^K}{d_s}\exp\left(\frac{-z^2}{2d_s^2}\right)$$

where K is the type of monomer bead; the term $f_s(x,y,K)$ adopts the values of either −1 or +1, depending on the value of K and the position of the bead. ΛN defines the strength of interaction between the surface and the bead; when a bead of type A is in a position preferable to type B, the overall energy contribution should be positive, and $\Lambda^A = -\Lambda^B$.

DOI: 10.1021/acsnano.8b08382
ACS Nano XXXX, XXX, XXX−XXX

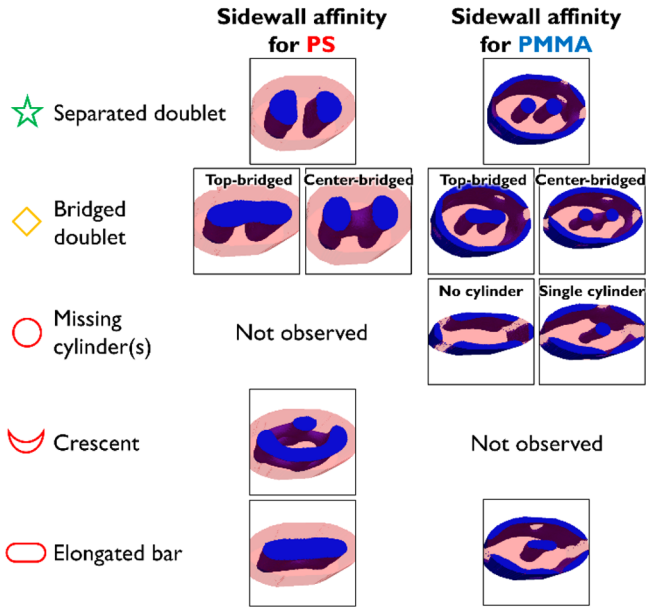

Figure 11. Images representative of stable morphologies resulting from MC simulations for PS-wetting and PMMA-wetting sidewall confinements, grouped into five main categories. Blue structures represent PMMA, and the red background corresponds to PS. It should be noted that these images are provided only for qualitative reference, since the aspect ratios of the images are adjusted to be the same even though the morphologies originate from confinements of different sizes.

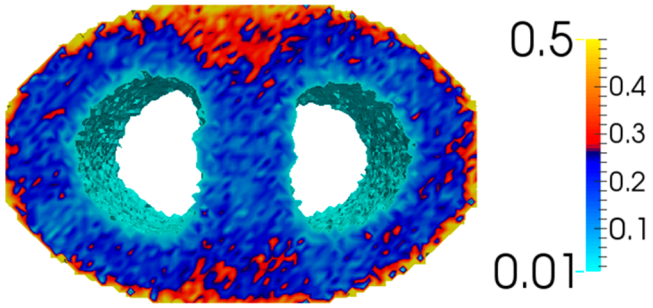

Figure 12. PS homopolymer density in a template $(2.2 \times 1.4\, L_0)$ with sidewall affinity for PS in which a separated doublet phase is predicted to be stable using PS-*b*-PMMA + 10% 10 kg mol^{-1} PS. Bright red regions at the upper and lower region of the template are indicative of homopolymer-enriched areas.

Lastly, z is the distance to the surface, and d_s is the decay length of the potential. Both the sidewall and the bottom surface contribute to a term of this form, with each parameter adopting (potentially) unique values. In this work, the value of Λ is set empirically by matching to the experimental results $-\Lambda N = -0.5$ for PMMA-wetting and $\Lambda N = 1.5$ for PS-wetting. In all cases, $\Lambda N = 0$ at the bottom surface. In order to utilize the hard wall potential described above, one must approximate the lateral hard wall as either being at the edge of the SOC dimensions (a slight overestimation) or at the edge of the polymer brush layer used for surface modification (a slight underestimation). As previously indicated, these polymer brushes will interdigitate with the block copolymer blend during self-assembly and as such do not correspond to the true confinement accessible to the block copolymer for assembly. For this reason, we have chosen to place the hard wall at the edge of the SOC dimensions.

The model is implemented in the context of a MC simulation. A MC cycle consists of either the attempted displacement of every bead or the attempted reptation of every chain. In each case, the randomly proposed positions are accepted with probability $p_{acc} = \min\left[1, \exp\left(\frac{-\Delta E}{k_B T}\right)\right]$. Thus, the simulations done here are in the NVT ensemble.

In this work, the stable morphology obtained after 100,000 MC cycles is represented. We note that, while the same names are used for some morphologies obtained from both PS-wetting and PMMA-wetting sidewall confinements, they should be regarded as different morphologies, as in all cases in PMMA-wetting sidewall confinements, the walls are covered in a layer of PMMA, which is never the case for PS-wetting sidewall confinements. The morphology visualizations in Figure 10 are density fields of an order parameter, Φ_1, calculated on a discretized grid.

$$\phi_1 = \frac{\phi_{PMMA} - \phi_{PS}}{\phi_{PMMA} + \phi_{PS}}$$

This parameter takes the value of 1 for a pure PMMA grid cell, −1 for a pure PS grid, and intermediate values for mixed regions. For clarity, these representative images are portrayed in solid color, with blue structures representing PMMA and the red background representing PS. For Figure 12, another order parameter is defined to allow clear visualization of the homopolymer density:

$$\phi_2 = \frac{\left(\frac{\phi_{homopolymer} - \phi_{copolymer}}{\phi_{homopolymer} + \phi_{copolymer}}\right) + \left(\frac{\phi_{homopolymer,bulk} - \phi_{copolymer,bulk}}{\phi_{homopolymer,bulk} + \phi_{copolymer,bulk}}\right)}{\left(\frac{\phi_{homopolymer,bulk} - \phi_{copolymer,bulk}}{\phi_{homopolymer,bulk} + \phi_{copolymer,bulk}}\right)}$$

This parameter takes on the value of 0 when the density of homopolymer in a grid cell is exactly the average homopolymer density, values below 0 when less than the average density, and values greater than zero when greater than the average density.

ASSOCIATED CONTENT

Supporting Information

The Supporting Information is available free of charge on the ACS Publications website at DOI: 10.1021/acsnano.8b08382.

Data on SEM signal intensity for Figures 4 and 5, SEM images for increased annealing times, the same SEM images as shown in Figures 4, 5, 7, and 9 but with larger field of view, and experimental process windows for doublets as a function of template area and pattern density (PDF)

AUTHOR INFORMATION

Corresponding Author

*E-mail: jan.doise@imec.be.

ORCID

Jan Doise: 0000-0002-9740-2668

Cody Bezik: 0000-0002-1940-4895

Juan J. de Pablo: 0000-0002-3526-516X

Present Address

⊥KLA Tencor/ICOS Belgium, Esperantolaan 8, 3001 Leuven, Belgium

Notes

The authors declare no competing financial interest.

ACKNOWLEDGMENTS

J.D. gratefully acknowledges the support of a Ph.D. stipend from the Agency for Innovation by Science and Technology (IWT). This work was supported by the U.S. Department of Energy, Office of Basic Energy Sciences, Division of Materials Science and Engineering. The collaboration between imec and the University of Chicago on copolymer design is funded by the

DOI: 10.1021/acsnano.8b08382
ACS Nano XXXX, XXX, XXX−XXX

Center for Hierarchical Materials Design (CHiMaD) and Mentor Graphics.

REFERENCES

(1) Herr, D. J. C. Directed Block Copolymer Self-Assembly for Nanoelectronics Fabrication. *J. Mater. Res.* **2011**, *26*, 122−139.

(2) Stoykovich, M. P.; Nealey, P. F. Block Copolymers and Conventional Lithography. *Mater. Today* **2006**, *9*, 20−29.

(3) Lu, W.; Lieber, C. M. Nanoelectronics from the Bottom Up. *Nat. Mater.* **2007**, *6*, 841−850.

(4) Stoykovich, M. P.; Müller, M.; Kim, S. O.; Solak, H. H.; Edwards, E. W.; de Pablo, J. J.; Nealey, P. F. Directed Assembly of Block Copolymer Blends into Nonregular Device-Oriented Structures. *Science* **2005**, *308*, 1442−1446.

(5) Winey, K. I.; Thomas, E. L.; Fetters, L. J. Swelling a Lamellar Diblock Copolymer with Homopolymer: Influences of Homopolymer Concentration and Molecular Weight. *Macromolecules* **1991**, *24*, 6182−6188.

(6) Mayes, A. M.; Russell, T. P.; Satija, S. K.; Majkrzak, C. F. Homopolymer Distributions in Ordered Block Copolymers. *Macromolecules* **1992**, *25*, 6523−6531.

(7) Matsen, M. W. Phase Behavior of Block Copolymer/Homopolymer Blends. *Macromolecules* **1995**, *28*, 5765−5773.

(8) Hashimoto, T.; Tanaka, H.; Hasegawa, H. Ordered Structure in Mixtures of a Block Copolymer and Homopolymers. 2. Effects of Molecular Weights of Homopolymers. *Macromolecules* **1990**, *23*, 4378−4386.

(9) Stuen, K. O.; Thomas, C. S.; Liu, G.; Ferrier, N.; Nealey, P. F. Dimensional Scaling of Cylinders in Thin Films of Block Copolymer−Homopolymer Ternary Blends. *Macromolecules* **2009**, *42*, 5139−5145.

(10) Liu, G.; Stoykovich, M. P.; Ji, S.; Stuen, K. O.; Craig, G. S. W.; Nealey, P. F. Phase Behavior and Dimensional Scaling of Symmetric Block Copolymer−Homopolymer Ternary Blends in Thin Films. *Macromolecules* **2009**, *42*, 3063−3072.

(11) Chevalier, X.; Nicolet, C.; Tiron, R.; Gharbi, A.; Argoud, M.; Couderc, C.; Fleury, G.; Hadziioannou, G.; Iliopoulos, I.; Navarro, C. Improvements of Self-Assembly Properties *via* Homopolymer Addition or Block-Copolymer Blends. In *Proceedings of SPIE*; Resnick, D. J., Bencher, C., Eds.; International Society for Optics and Photonics: Bellingham WA, 2014; p 90490T.

(12) Kim, B. H.; Park, S. J.; Jin, H. M.; Kim, J. Y.; Son, S.-W.; Kim, M.-H.; Koo, C. M.; Shin, J.; Kim, J. U.; Kim, S. O. Anomalous Rapid Defect Annihilation in Self-Assembled Nanopatterns by Defect Melting. *Nano Lett.* **2015**, *15*, 1190−1196.

(13) Jeon, H. U.; Jin, H. M.; Kim, J. Y.; Cha, S. K.; Mun, J. H.; Lee, K. E.; Oh, J. J.; Yun, T.; Kim, J. S.; Kim, S. O. Electric Field Directed Self-Assembly of Block Copolymers for Rapid Formation of Large-Area Complex Nanopatterns. *Mol. Syst. Des. Eng.* **2017**, *2*, 560−566.

(14) Jin, H. M.; Lee, S. H.; Kim, J. Y.; Son, S.-W.; Kim, B. H.; Lee, H. K.; Mun, J. H.; Cha, S. K.; Kim, J. S.; Nealey, P. F.; Lee, K. J.; Kim, S. O. Laser Writing Block Copolymer Self-Assembly on Graphene Light-Absorbing Layer. *ACS Nano* **2016**, *10*, 3435−3442.

(15) Shin, D. O.; Jeong, J.-R.; Han, T. H.; Koo, C. M.; Park, H.-J.; Lim, Y. T.; Kim, S. O. A Plasmonic Biosensor Array by Block Copolymer Lithography. *J. Mater. Chem.* **2010**, *20*, 7241.

(16) Cheng, J. Y.; Sanders, D. P.; Truong, H. D.; Harrer, S.; Friz, A.; Holmes, S.; Colburn, M.; Hinsberg, W. D. Simple and Versatile Methods to Integrate Directed Self-Assembly with Optical Lithography Using a Polarity-Switched Photoresist. *ACS Nano* **2010**, *4*, 4815−4823.

(17) Latypov, A.; Coskun, T. H.; Garner, G.; Preil, M.; Schmid, G.; Xu, J.; Zou, Y. Simulations of Spatial DSA Morphology, DSA-Aware Assist Features and Block Copolymer-Homopolymer Blends. *Proc. SPIE* **2014**, *9049*, 904908.

(18) Doise, J.; Bekaert, J.; Chan, B. T.; Hori, M.; Gronheid, R. *Via* Patterning in the 7-Nm Node Using Immersion Lithography and Graphoepitaxy Directed Self-Assembly. *J. Micro/Nanolithogr., MEMS, MOEMS* **2017**, *16*, 023506.

(19) Kato, H.; Seino, Y.; Yonemitsu, H.; Sato, H.; Kanno, M.; Kobayashi, K.; Kawanishi, A.; Imamura, T.; Omura, M.; Nakamura, N.; Azuma, T. Sub-30nm *via* Interconnects Fabricated Using Directed Self-Assembly. *Microelectron. Eng.* **2013**, *110*, 152−155.

(20) Yi, H.; Bao, X.; Zhang, J.; et al. Flexible Control of Block Copolymer Directed Self-Assembly Using Small, Topographical Templates: Potential Lithography Solution for Integrated Circuit Contact Hole. *Adv. Mater.* **2012**, *24*, 3107−3114.

(21) Torres, J.; Sakajiri, K.; et al. Physical Verification and Manufacturing of Contact/*via* Layers Using Grapho-Epitaxy DSA Processes. *Proc. SPIE* **2014**, *9053*, 90530R.

(22) Bekaert, J.; Doise, J.; Gronheid, R.; Ryckaert, J.; Vandenberghe, G.; Fenger, G.; Her, Y. J.; Cao, Y. N7 Logic *via* Patterning Using Templated DSA: Implementation Aspects. *Proc. SPIE* **2015**, *9658*, 965804.

(23) Yi, H.; Bao, X.-Y.; Tiberio, R.; Wong, H.-S. P. A General Design Strategy for Block Copolymer Directed Self-Assembly Patterning of Integrated Circuits Contact Holes Using an Alphabet Approach. *Nano Lett.* **2015**, *15*, 805−812.

(24) Doise, J.; Bekaert, J.; Chan, B. T.; Gronheid, R.; Cao, Y.; Hong, S.; Lin, G.; Fishman, D.; Chakk, Y.; Marzook, T. Implementation of Surface Energy Modification in Graphoepitaxy Directed Self-Assembly for Hole Multiplication. *J. Vac. Sci. Technol., B: Nanotechnol. Microelectron.: Mater., Process., Meas., Phenom.* **2015**, *33*, 06F301.

(25) Gronheid, R.; Boeckx, C.; Doise, J.; Bekaert, J.; Karageorgos, I.; Ruckaert, J.; Chan, B. T.; Lin, C.; Zou, Y. EUV Patterned Templates with Grapho-Epitaxy DSA at the N5/N7 Logic Nodes. *Proc. SPIE* **2016**, *97761*, 97761W.

(26) Doise, J.; Bekaert, J.; Chan, B. T.; Hong, S.; Lin, G.; Gronheid, R. Influence of Template Fill in Graphoepitaxy Directed Self-Assembly. *J. Micro/Nanolithogr., MEMS, MOEMS* **2016**, *15*, 031603.

(27) Fox, T. G.; Flory, P. J. The Glass Temperature and Related Properties of Polystyrene. Influence of Molecular Weight. *J. Polym. Sci.* **1954**, *14*, 315−319.

(28) Fox, T. G. Influence of Diluent and of Copolymer Composition on the Glass Transition Temperature of a Polymer System. *Bull. Am. Phys. Soc.* **1956**, *1*, 123.

(29) Legrand, D. G.; Gaines, G. L. The Molecular Weight Dependence of Polymer Surface Tension. *J. Colloid Interface Sci.* **1969**, *31*, 162−167.

(30) Detcheverry, F. A.; Pike, D. Q.; Nealey, P. F.; Müller, M.; de Pablo, J. J. Monte Carlo Simulation of Coarse Grain Polymeric Systems. *Phys. Rev. Lett.* **2009**, *102*, 197801.

(31) Hur, S.-M.; Thapar, V.; Ramírez-Hernández, A.; Khaira, G.; Segal-Peretz, T.; Rincon-Delgadillo, P. A.; Li, W.; Müller, M.; Nealey, P. F.; de Pablo, J. J. Molecular Pathways for Defect Annihilation in Directed Self-Assembly. *Proc. Natl. Acad. Sci. U. S. A.* **2015**, *112*, 14144−14149.

(32) Bezik, C. T.; Garner, G. P.; de Pablo, J. J. Mechanisms of Directed Self-Assembly in Cylindrical Hole Confinements. *Macromolecules* **2018**, *51*, 2418.

(33) Okabe, K.; Yi, H.; Tung, M. C.; Tiberio, R.; Bekaert, J.; Gronheid, R.; Wong, H.-S. P. Cross-Sectional Imaging of Directed Self-Assembly Block Copolymers. *Proc. SPIE* **2015**, 942318.

(34) Matsen, M. W.; Schick, M. Stable and Unstable Phases of a Diblock Copolymer Melt. *Phys. Rev. Lett.* **1994**, *72*, 2660−2663.

(35) Fredrickson, G. H. *The Equilibrium Theory of Inhomogeneous Polymers*; Oxford Science Publications: Oxford, 2005.

(36) Detcheverry, F. A.; Kang, H.; Daoulas, K. C.; Müller, M.; Nealey, P. F.; de Pablo, J. J. Monte Carlo Simulations of a Coarse Grain Model for Block Copolymers and Nanocomposites. *Macromolecules* **2008**, *41*, 4989−5001.

(37) Detcheverry, F. A.; Liu, G.; Nealey, P. F.; de Pablo, J. J. Interpolation in the Directed Assembly of Block Copolymers on Nanopatterned Substrates: Simulation and Experiments. *Macromolecules* **2010**, *43*, 3446−3454.

DOI: 10.1021/acsnano.8b08382
ACS Nano XXXX, XXX, XXX−XXX